Multi-Scale Colour Completed Local Binary Patterns for Scene and Event Sport Image Categorisation

Taha H. Rassem, *Member, IAENG,* Bee Ee Khoo, Nasrin M. Makbol, and AbdulRahman A. Alsewari

Abstract—**The Local Binary Pattern (LBP) texture descriptor and some of its variant descriptors have been successfully used for texture classification and for a few other tasks such as face recognition, facial expression, and texture segmentation. However, these descriptors have been barely used for image categorisation because their calculations are based on the gray image and they are only invariant to monotonic light variations on the gray level. These descriptors ignore colour information despite their key role in distinguishing the objects and the natural scenes. In this paper, we enhance the Completed Local Binary Pattern (CLBP), an LBP variant with an impressive performance on texture classification. We propose five multi-scale colour CLBP (CCLBP) descriptors by incorporating five different colour information into the original CLBP. By using the Oliva and Torralba (OT8) and Event sport datasets, our results attest to the superiority of the proposed CCLBP descriptors over the original CLBP in terms of image categorisation.**

Index Terms—**Local Binary Pattern (LBP), Texture Descriptors, Completed Local Binary Pattern (CLBP), colour CLBP (CCLBP), Image Categorisation.**

I. Introduction

TEXTURE features are vital in many of today's applications such as human detectors [1], face recognition [2], [3], image retrieval [4], [5], finger detection [6], texture segmentation [7], and visual object recognition [8]–[10]. Previous literature identifies many textures feature algorithms for robust and distinctive texture features. Zhang et al. [11] classified the texture feature algorithm methods into three categories, namely, the statistical algorithm methods, the model-based methods, and structural methods. Many studies have comprehensively reviewed these texture algorithm methods [11], [12].

In 1996, Ojala et al. [13] calculated the absolute difference between the gray level of the centre pixel of a specific local pattern and its neighbours to construct a histogram representing the image texture. This absolute difference, instead of the magnitude, was subsequently used to construct the Local Binary Pattern (LBP) texture descriptor [14]. LBP has become an interesting research topic for many computer vision researchers for its ability to discern the microstructures of an image, such as edges, lines and spots. LBP has been proposed for rotation invariant texture classification and has been extended for several applications, such as face recognition [15], and image retrieval [5].

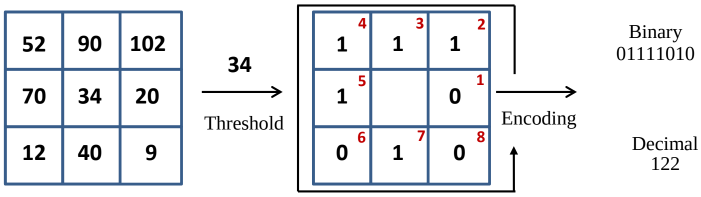

Fig. 1. LBP operator.

Fig. 1 shows two steps of the LBP, namely, the thresholding step and the encoding step. The former compares the values of the central pixel with the values of all neighbouring pixels to convert the values of the neighbouring pixels into binary values (0 or 1). The latter encodes and converts these binary values into decimal numbers to characterise a structural pattern.

Many LBP variants have been suggested to increase the discriminating property of the texture feature extraction. These variants include the Center-Symmetric Local Binary Pattern (CS-LBP) [16], the Dominant LBP (DLBP) [17], the Local Ternary Pattern (LTP) [18], the Completed Modelling of LBP (CLBP) [19], and Completed Ternary Pattern (CLTP) [20], and Local Orientation Adaptive Descriptor (LOAD) [21]

Although many texture features have been successfully used for many tasks such as texture classification, face recognition, facial expression and texture segmentation, these features are rarely used for visual object class recognition. Although colour is important information in visual object recognition, many texture features do not consider the colour information because many of their calculations are based on the gray scale image and texture features are only invariant to monotonic light variations on the gray level. Incorporating colour into the texture operators enhance the operators' photometric invariance and discriminating properties [22], [23], as well as helping them to distinguish the objects and the natural scenes.

Zhu et al. [22] proposed and used six colour LBP for visual object class recognition. The multi-scale LBP histogram was extracted from each colour channel, and then

Manuscript received November 11, 2016; revised March 11, 2017; accepted May 03, 2017. This work is supported by the Universiti Malaysia Pahang (UMP) via Research Grant UMP- IBM Centre of Excellence-RDU160349.

Taha H. Rassem is senior lecturer with Faculty of Computer Systems and Software Engineering, and IBM Centre of Excellence, Universiti Malaysia Pahang, Malaysia, e-mail: tahahussein@ump.edu.my

Bee Ee Khoo is an associate professor with School of Electrical and Electronic Engineering, Universiti Sains Malaysia, email: Beekhoo@usm.my

Nasrin M. Makbol is an assistant professor with Faculty of Computer Science and Engineering, Hodeidah University, Yemen, postdoctoral fellow at with School of Electrical and Electronic Engineering, Universiti Sains Malaysia, email: nasrin_makbol@usm.my

AbdulRahman A. Alsewari is senior lecturer with Faculty of Computer Systems and Software Engineering, and IBM Centre of Excellence, Universiti Malaysia Pahang, Malaysia, email: alsewari@ump.edu.my

all the colour and multi-scale histograms for the colour space channels were concatenated to construct the final LBP histogram. Banerji et al. [23] also incorporated LBP with different colour information for visual object class recognition. In [24], the PHOG descriptor was combined with the colour LBP to achieve high quality recognition results. Fig. 2 shows the calculation of the colour LBP.

Inspired by the CLBP texture descriptor, five novel multi-scale colour CLBP texture descriptors (CCLBP) are proposed in this paper to enhance the photometric invariance and discriminative power of the original CLBP. Guo et al. [19] proposed a Completed Modelling of LBP (CLBP) by comparing both the sign and the magnitude of the pattern's central gray level value with its neighbours and by combining them with all central values of the patterns. The sign difference, the magnitude difference, and the threshold of the central gray values of the patterns are combined in different ways to construct three CLBP operators [19], namely, $CLBP\_S$, $CLBP\_M$ and $CLBP\_C$, respectively, which are, in turn, calculated based on five different colour spaces, namely, RGB, HSV, Opponent colour, Transformed-colour, and Ohta colour spaces. These descriptors are then combined to construct the CCLBP descriptor. The performances of the proposed CCLBP descriptors are evaluated and analysed experimentally for image categorisation.

The rest of this paper is organised as follows. Sections II and III briefly review LBP and the Completed Local Binary Pattern (CLBP) texture descriptors, respectively. Section IV presents the proposed CCLBP descriptors. Section V discusses the experimental results of the OT8 and the Event sport datasets. Lastly, Section VI concludes the paper.

II. Local Binary Pattern (LBP)

The LBP calculation can be described mathematically as follows:

$$LBP_{P,R} = \sum_{p=0}^{P-1} 2^p s(i_p - i_c), \quad s(x) = \begin{cases} 1, & x \geq 0, \\ 0, & x < 0, \end{cases} \tag{1}$$

where i_c and $i_p (p = 0, , P-1)$ denote the gray values of the centre pixel and the neighbour pixel on a circle of radius R, respectively, and P denotes the number of neighbours. Bilinear interpolation estimation method is used to identify the neighbours that do not lie in the exact centre of the pixels.

Ojala et al. [14] also improved the original LBP into the rotation invariant LBP ($LBP^{ri}_{P,R}$) and the uniform rotation invariant LBP ($LBP^{riu2}_{P,R}$). After encoding these LBP types, i.e., LBP, $LBP^{ri}_{P,R}$ and $LBP^{riu2}_{P,R}$, the descriptor histogram is constructed based on the following equation:

$$H(k) = \sum_{i=0}^{I} \sum_{j=0}^{J} f(LBP_{P,R}(i,j), k), \quad k \in [0, K],$$
$$f(x,y) = \begin{cases} 1, & x = y, \\ 0, & otherwise, \end{cases} \tag{2}$$

where K is the maximal LBP pattern value.

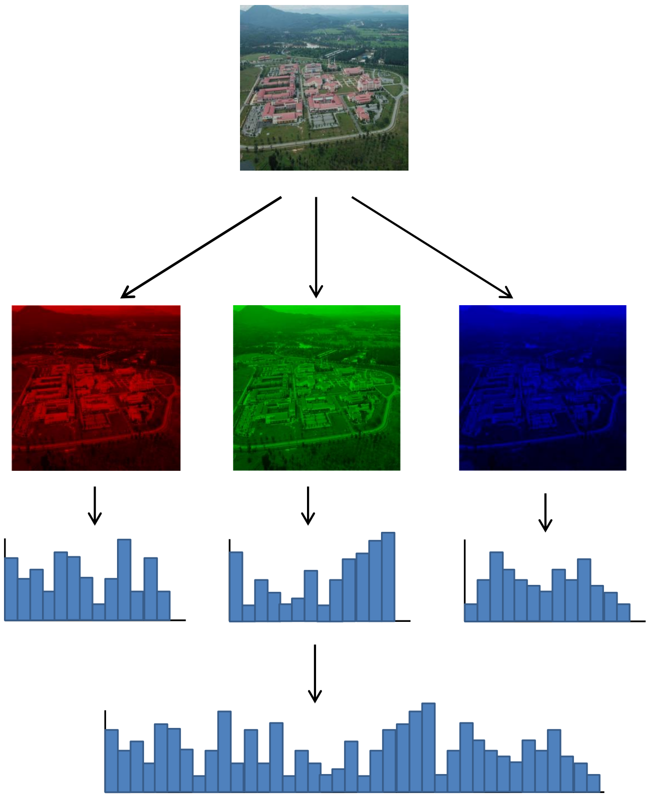

Fig. 2. Colour LBP calculation.

III. Completed Local Binary Pattern (CLBP)

Fig. 3 shows the decomposition of the image local difference into two complementary components, namely, the sign component s_p and the magnitude component m_p which can be mathematically expressed as follows.

$$s_p = s(i_p - i_c), \quad m_p = |i_p - i_c| \tag{3}$$

s_p is used to construct $CLBP\_S$, while m_p is used to construct $CLBP\_M$. These two operators are mathematically expressed as follows:

$$CLBP\_S_{P,R} = \sum_{p=0}^{P-1} 2^p s(i_p - i_c), \quad s_p = \begin{cases} 1, & i_p \geq i_c, \\ 0, & i_p < i_c, \end{cases} \tag{4}$$

$$CLBP\_M_{P,R} = \sum_{p=0}^{P-1} 2^p t(m_p, c),$$
$$t(m_p, c) = \begin{cases} 1, & |i_p - i_c| \geq c, \\ 0, & |i_p - i_c| < c, \end{cases} \tag{5}$$

where i_c, i_p, R, and P are defined in (1), while c denotes the mean value of m_p in the entire image.

$CLBP\_S$ is equivalent to LBP, whereas $CLBP\_M$ measures the local variance of the magnitude. Guo et al. constructed the CLBP-Centre ($CLBP\_C$) by thresholding the values of each pattern using the average gray level of the entire image. $CLBP\_C$ is expressed mathematically as follows:

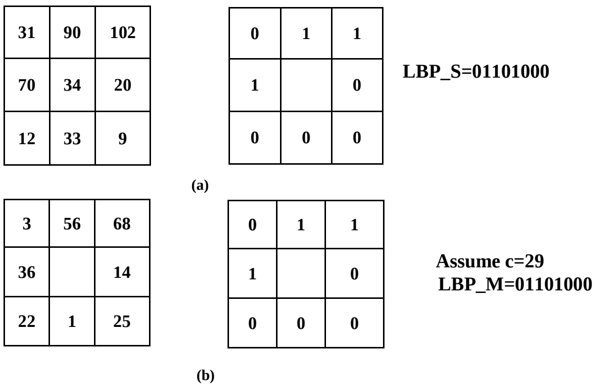

Fig. 3. A 3×3 sample pattern (a) sign component (LBP_S code) (b) magnitude components (LBP_M code (assume threshold = 29)).

$$CLBP\_C_{P,R} = t(i_c, c_I) \tag{6}$$

where i_c denotes the gray value of the centre pixel of the pattern and c_I denotes the average gray level of the whole image. Guo et al. [19] combined the CLBP operators into joint or hybrid distributions. They combined $CLBP\_S$ with $CLBP\_M$ in two ways. Firstly, their histogram is concatenated to construct $CLBP\_S\_M$. Secondly, the $2D$ joint histogram known as $CLBP\_S/M$, is calculated.

$CLBP\_C$ is also combined with $CLBP\_S$ and $CLBP\_M$ in two ways. Firstly, both operators are combined to form a $3D$ joint histogram, known as $CLBP\_S/M/C$. Secondly, $CLBP\_C$ is combined jointly with the $CLBP\_S$ or $CLBP\_M$ to construct two $2D$ joint histograms, namely, $CLBP\_S/C$ or $CLBP\_M/C$, respectively. These histograms are then converted into $1D$ histograms and are concatenated with $CLBP\_M$ or $CLBP\_S$ to build the final histogram, either known as $CLBP\_M\_S/C$ or $CLBP\_S\_M/C$.

In [19], the rotation invariant LBP ($LBP^{riu2}_{P,R}$) is used to construct the $CLBP^{riu2}_{P,R}$ operators. The $CLBP^{riu2}_{P,R}$ is simplified in this paper as $CLBP_{P,R}$ as well as the proposed CCLBP operators.

IV. Proposed Colour Completed Local Binary Pattern (CCLBP)

This section calculates $CCLBP\_S$, $CCLBP\_M$ and $CCLBP\_C$ based on five different colour spaces, namely, RGB, HSV, Opponent colour, Transformed-colour and Ohta colour spaces. These operators are then combined to construct the CCLBP descriptor.

A. Model Analysis for Illumination Changes and Photometric Transformations

To analyse the illumination changes and photometric transformations of the proposed colour CLBP, the diagonal model and diagonal-offset model are used [25]–[27]. The first model is expressed by Equation (7) while the latter model is expressed by Equation (8).

$$\begin{pmatrix} R^c \\ G^c \\ B^c \end{pmatrix} = \begin{pmatrix} a & 0 & 0 \\ 0 & b & 0 \\ 0 & 0 & c \end{pmatrix} \begin{pmatrix} R^u \\ G^u \\ B^u \end{pmatrix} \tag{7}$$

$$\begin{pmatrix} R^c \\ G^c \\ B^c \end{pmatrix} = \begin{pmatrix} a & 0 & 0 \\ 0 & b & 0 \\ 0 & 0 & c \end{pmatrix} \begin{pmatrix} R^u \\ G^u \\ B^u \end{pmatrix} + \begin{pmatrix} o_1 \\ o_2 \\ o_3 \end{pmatrix} \tag{8}$$

Using these two models, Van de Sande et al. [26] identified five different changes to examine some colour SIFT descriptors. These changes, including the light intensity variations, light intensity shifts, light intensity variations and shifts, light colour variations and light colour variations and shifts. From Equation (7), the light intensity change can be expressed when all channels image values are changed by a constant factor; i.e., $a = b = c$. With respect to the intensity, invariant to the light intensity variations that mean the descriptor is scale invariant.

$$\begin{pmatrix} R^c \\ G^c \\ B^c \end{pmatrix} = \begin{pmatrix} a & 0 & 0 \\ 0 & a & 0 \\ 0 & 0 & a \end{pmatrix} \begin{pmatrix} R^u \\ G^u \\ B^u \end{pmatrix} \tag{9}$$

In light intensity shift, the image values are changed by equal offset value (shift value); i.e., ($O_1 = O_2 = O_3$ and $a = b = c = 1$). With respect to the intensity, invariant to the light intensity shifts means that the descriptor is shift invariant.

$$\begin{pmatrix} R^c \\ G^c \\ B^c \end{pmatrix} = \begin{pmatrix} R^u \\ G^u \\ B^u \end{pmatrix} + \begin{pmatrix} o_1 \\ o_1 \\ o_1 \end{pmatrix} \tag{10}$$

In the third model, the image values are changed by both the above types of changes; i.e., light intensity changes and shifts, as expressed in the following model.

$$\begin{pmatrix} R^c \\ G^c \\ B^c \end{pmatrix} = \begin{pmatrix} a & 0 & 0 \\ 0 & a & 0 \\ 0 & 0 & a \end{pmatrix} \begin{pmatrix} R^u \\ G^u \\ B^u \end{pmatrix} + \begin{pmatrix} o_1 \\ o_1 \\ o_1 \end{pmatrix} \tag{11}$$

The remaining models are light colour variations and light colour variations and shifts. In the former model, the image values in each channel are changed independently; i.e., $a \neq b \neq c$, as expressed in Equation (7). While in the latter model, the image values in each channel are changed and shifted independently; i.e., $a \neq b \neq c$ and $O_1 \neq O_2 \neq O_3$, as expressed in Equation (8).

1) RGB-CCLBP: The RGB-CCLBP operators are obtained by computing CLBP independently in all three channels of the RGB colour space and by concatenating the results together. Similar to the original LBP, the RGB-CCLBP is also invariant to monotonic light intensity change and has no more invariant properties.

2) HSV-CCLBP: The HSV CCLBP operators are obtained by computing CLBP independently in all three channels of the HSV colour space and by concatenating the results together. Van De Weijer et al. [28] proved the H colour model (Hue) in HSV colour space has invariant property against the light intensity changes and shifts; i.e., scale-invariant and shift-invariant with respect to light intensity. However, due the combination of Hue with the remaining information; i.e., saturation and value, the HSV-CCLBP has no invariant properties.

3) Opponent CCLBP: The Opponent CCLBP operators are obtained by computing CLBP independently in all three channels of the Opponent colour space and by concatenating the results together. The Opponent colour channels can be described by the following equation:

$$\begin{pmatrix} O_1 \\ O_2 \\ O_3 \end{pmatrix} = \begin{pmatrix} \frac{R-G}{\sqrt{2}} \\ \frac{R+G-2B}{\sqrt{6}} \\ \frac{R+G+B}{\sqrt{(3)}} \end{pmatrix} \tag{12}$$

where O_1 and O_2 represent the colour information while O_3 represents the intensity information.

Based on Equation (12), the O_1 and O_2 has shift-invariant while no invariant properties for the intensity channel O_3. So, the Opponent CCLBP has invariant property against light intensity changes.

4) Transformed CCLBP: The Transformed-CCLBP is obtained by computing CLBP independently in all three channels of the Transformed colour space and by concatenating the results together. The Transformed colour channels can be described by the following equation:

$$\begin{pmatrix} R' \\ G' \\ B' \end{pmatrix} = \begin{pmatrix} \frac{R-\mu_R}{\sigma_R} \\ \frac{G-\mu_G}{\sigma_G} \\ \frac{B-\mu_B}{\sigma_B} \end{pmatrix} \tag{13}$$

where μ_R, μ_G and μ_B are the mean values of R ,G and B channels, respectively, and σ_R, σ_G and σ_B are the standard deviation of each channel.

The Transformed CCLBP has invariant property against the light intensity changes and shifts (scale-invariant and shift-invariant). This is due to the subtraction and the normalisation as shown in Equation (13). This descriptor is also invariant to light colour change and shift because the Transformed colour space has these invariant properties [26], [29].

5) Ohta CCLBP: The Ohta CCLBP is obtained by computing CLBP independently in all three channels of the Ohta colour space [30] and by concatenating the results together. The Ohta colour channels can be described by the following equation:

$$\begin{pmatrix} I_1 \\ I_2' \\ I_3' \end{pmatrix} = \begin{pmatrix} \frac{R+G+B}{3} \\ R-B \\ \frac{2G-R-B}{2} \end{pmatrix} \tag{14}$$

where I_1 represents the intensity component while ${I_2}'$ and ${I_3}'$ represent the approximate orthogonal colour components. The Ohta colour space (only I_2 and I_2) has only the shift invariant property. This is due to the subtraction as shown in following equation:

$$\begin{pmatrix} I_2' \\ I_3' \end{pmatrix} = \begin{pmatrix} R-B \\ \frac{2G-R-B}{2} \end{pmatrix} = \begin{pmatrix} (R'+o_1)-(B'+o_1) \\ \frac{2(G'+o_1)-(R'+o_1)-(B'+o_1)}{2} \end{pmatrix} = \begin{pmatrix} R'-B' \\ \frac{2G'-R'-B'}{2} \end{pmatrix} \tag{15}$$

The Ohta colour has not invariant to the light colour changes and shifts, and to the light intensity changes (scale invariant). So, the Ohta-CCLBP has the same properties.

B. Mathematical Models of CCLBP

Similar to Equations (4), (5) and (6), CCLBP operators can be calculated in each channel as follows:

$$(CCLBP\_S_{P,R})^{C1} = \sum_{p=0}^{P-1} 2^p s(i_p - i_c), \quad s_p = \begin{cases} 1, & i_p \geq i_c, \\ 0, & i_p < i_c, \end{cases} \tag{16}$$

$$(CCLBP\_S_{P,R})^{C2} = \sum_{p=0}^{P-1} 2^p s(i_p - i_c), \quad s_p = \begin{cases} 1, & i_p \geq i_c, \\ 0, & i_p < i_c, \end{cases} \tag{17}$$

$$(CCLBP\_S_{P,R})^{C3} = \sum_{p=0}^{P-1} 2^p s(i_p - i_c), \quad s_p = \begin{cases} 1, & i_p \geq i_c, \\ 0, & i_p < i_c, \end{cases} \tag{18}$$

where $C1$, $C2$, and $C3$ are the colour space channels. The final $CCLBP\_S$ can be calculated as follows.

$$CCLBP\_S_{P,R} = [(CLBP\_S_{P,R})^{C1} \quad (CLBP\_S_{P,R})^{C2} \quad (CLBP\_S_{P,R})^{C3}] \tag{19}$$

Similar to equation (5), the $CCLBP\_M$ can be calculated as follows:

$$CCLBP\_M_{P,R} = [(CLBP\_M_{P,R})^{C1} \quad (CLBP\_M_{P,R})^{C2} \quad (CLBP\_M_{P,R})^{C3}] \tag{20}$$

To construct the remaining operators, the $CCLBP\_S$, $CCLBP\_M$ and $CCLBP\_C$ for each colour channel are combined jointly or hybridized similar to the method that are explained in Section III. The final CCLBP operators, which are the concatenation of all colour channel operators, can be mathematically described as follows:

$$CCLBP\_S/M_{P,R} = [(CLBP\_S/M_{P,R})^{C1}(CLBP\_S/M_{P,R})^{C2}(CLBP\_S/M_{P,R})^{C3}] \tag{21}$$

$$CCLBP\_S\_M_{P,R} = [(CLBP\_S\_M_{P,R})^{C1}(CLBP\_S\_M_{P,R})^{C2}(CLBP\_S\_M_{P,R})^{C3}] \tag{22}$$

$$CCLBP\_M/C_{P,R} = [(CLBP\_M/C_{P,R})^{C1}(CLBP\_M/C_{P,R})^{C2}(CLBP\_M/C_{P,R})^{C3}] \tag{23}$$

$$CCLBP\_S\_M/C_{P,R} = [(CLBP\_S\_M/C_{P,R})^{C1}(CLBP\_S\_M/C_{P,R})^{C2}(CLBP\_S\_M/C_{P,R})^{C3}] \tag{24}$$

$$CCLBP\_S/M/C_{P,R} = [(CLBP\_S/M/C_{P,R})^{C1}(CLBP\_S/M/C_{P,R})^{C2}(CLBP\_S/M/C_{P,R})^{C3}] \tag{25}$$

V. Experiments and discussion

Experiments are performed to evaluate the proposed CCLBP. The OT8 and the Event sport datasets are used in these experiments.

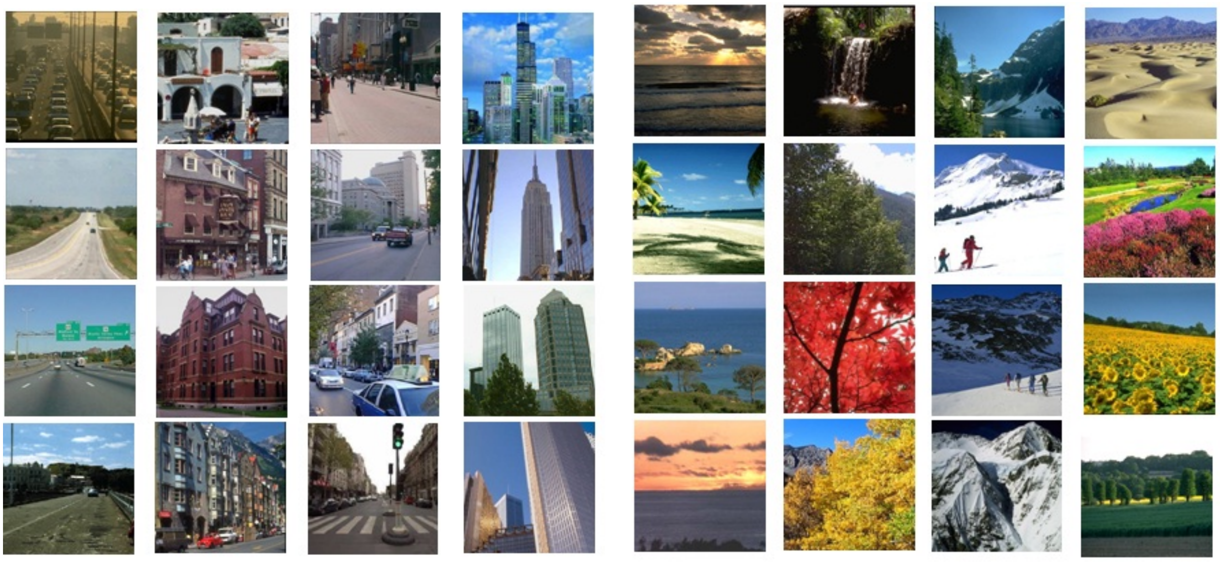

(a) OT Man-Made images (columns from left to right; highway, inside city, street and tall building)

(b) OT Natural images (columns from left to right; coast, forest, mountain and open city)

Fig. 4. Some images from Oliva & Torralba (OT) dataset.

A. Dissimilarity Measuring Framework

Several metrics are proposed to measure the dissimilarity between the two histograms, such as log-likelihood ratio, histogram intersection, and chi-square statistic. Similar to [19], these experiments use the chi-square statistic. The χ^2 distance between two histograms $H = h_i$ and $K = k_i$ (where $(i = 1, 2, 3, ...B)$) can be mathematically described as follows:

$$Dissimilarity_{\chi^2}(H, K) = \sum_{i=1}^{B} \frac{(h_i - k_i)^2}{h_i + k_i} \qquad (26)$$

These experiments use the nearest neighbourhood classifier for classification.

B. Experimental Results on OT8 Scene Dataset

The Oliva & Torralba dataset (OT8) has a total 2,688 colour images [32]. The dataset contains eight categories, namely, coast, forest, mountain, open country, highway, inside city, tall building, and street. These images are in JPG format and have an average size of 265 × 265 pixels. Figure 4 shows some examples of OT8 images. The OT8 scene dataset is used in these experiments to evaluate the proposed CCLBP and to compare its performance with the gray CLBP under various training images. In each class, $N = (10, 30, 40, 50, 100, 150, 200)$ is used as training images, while the remaining images are used as testing images. The final classification accuracy is determined by the average percentage over a hundred random splits. The comparison is performed on different texture patterns, namely, ($P = 8$ and $R = 1$), ($P = 16$ and $R = 2$), and ($P = 24$ and $R = 3$). These patterns are shown in Fig. 5. Figures 7, 8, and 9 exhibit the performances of the gray CLBP and the proposed CCLBP operators of these texture patterns.

Figs. 7(a) to 7(f) exhibit the performances of the texture operators of the $R = 1$ and $P = 8$ texture pattern. The following observations can be made based on these figures. Firstly, the gray $CLBP\_S$ has a better classification performance than $CCLBP\_S$. Secondly, gray $CLBP\_M$ operators are approximately similar to all $CCLBP\_M$ operators in terms of performance, except for the Opponent $CCLBP\_M$ operator. Thirdly, aside from the Opponent CCLBP operators, all remaining CCLBP operators have outperformed the gray CLBP operators. Finally, all Opponent CCLBP operators have the worst classification performances. The Transformed $CCLBP\_S/M/C$ operator has achieved the best classification accuracy, which has reached up to 58.49%.

Figs 8(a) to 8(f) show the performances of the texture operators of the $R = 2$ and $P = 16$ texture pattern. The following observations can be obtained from these figures. Firstly, the gray $CLBP\_S$ and $CLBP\_M$ operators have exhibited better performance than other $CCLBP\_S$ and $CCLBP\_M$ operators. Secondly, aside from the Opponent CCLBP operators, all remaining CCLBP operators have outperformed the gray CLBP operators. Finally, similar to the performance of the Opponent CCLBP operators when $R = 1$ and $P = 8$, these operators have exhibited the worst performance except in Fig. 8(f) where the Opponent $CCLBP\_S/M/C$ has outperformed the gray $CLBP\_S/M/C$ as the number of training images was increased. The RGB $CCLBP\_S/M/C$ operator has achieved the best classification accuracy, achieving up to 58.07%. Figs. 9(a) to 9(f) show the performances of the texture operators of the $R = 3$ and $P = 24$ texture pattern. The following observations can be made from these figures. Firstly, the gray $CLBP\_S$ and $CLBP\_M$ operators have a better performance than the other $CCLBP\_S$ and $CCLBP\_M$ operators. Secondly, the remaining CCLBP operators have outperformed their corresponding gray CLBP operators. As shown in Figs. 9(d) and 9(e), the performances of the Opponent $CCLBP\_S\_M/C$ and the Opponent $CCLBP\_S/M$ improved upon increasing the number of training images. The Opponent $CCLBP\_S/M$ has achieved the best classification accuracy, which has reached up to 54.17%. Lastly, $CCLBP\_M/C$, $CCLBP\_S\_M/C$, $CCLBP\_S/M$ and $CCLBP\_S/M/C$ operators have all

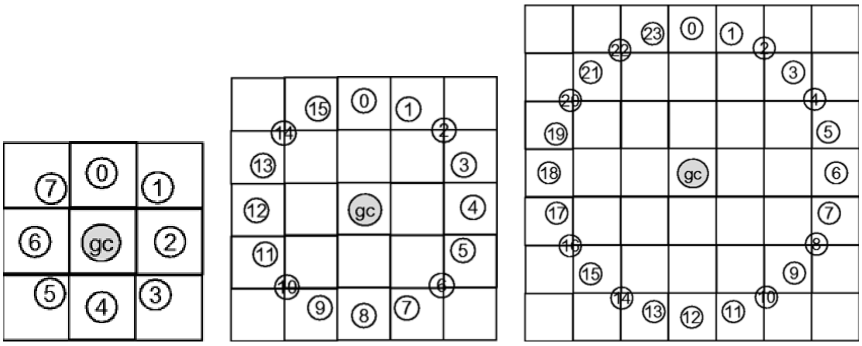

(a) P=8, R=1 (b) P=16, R=2 (c) P=24, R=3

Fig. 5. Texture pattern types [31].

(a) Badminton.

(b) Croquet.

(c) Bocce.

(d) Polo.

(e) RockClimbing.

(f) Rowing.

(g) Sailing.

(h) Snowboarding.

Fig. 6. Some images from Event sport dataset.

outperformed the gray CLBP operators. The Transformed $CCLBP\_S/M/C$ operator has achieved the best classification accuracy, achieving up to 57.25%. Generally speaking, the performances of CCLBP operators have outperformed the gray CLBP operators. Aside from the Opponent CCLBP operators, the performances of all CCLBP operators are approximately the same. Table I shows the classification accuracy results on OT8 database in details.

C. Experimental Results on Event sport Dataset

The Event sport dataset has eight categories, namely, rowing, badminton, polo, bocce, snow boarding, croquet, sailing, and rock climbing [33]. Figure 6 shows some examples of Event sport images. Similar to the OT8 datasets, the Event sport dataset is used to evaluate the proposed CCLBP and to compare its performance with the gray CLBP under various numbers of training images. In each class $N = (5, 10, 20, 30, 40, 50, 60)$ is used as the training images, while the remaining images are used as testing images. The final classification accuracy is determined by the average percentage over a hundred random splits. The comparison is performed on different texture patterns, namely, ($P = 8$ and $R = 1$), ($P = 16$ and $R = 2$), and ($P = 24$ and $R = 3$). Figs. 10, 11 and 12 show the performances of the gray CLBP and the proposed CCLBP operators.

Figs. 10(a) to 10(f) present the performances of the texture operators of the $R = 1$ and $P = 8$ texture pattern. The following observations can be formulated based on these figures. Firstly, Opponent $CCLBP\_S$ and Opponent $CCLBP\_M$ have performed the worst, whereas the Transformed $CCLBP\_S/M/C$, HSV $CCLBP\_S/M/C$ and RGB $CCLBP\_S/M/C$ have achieved top-ranking performances. Secondly, unlike the other CLBP operators, the

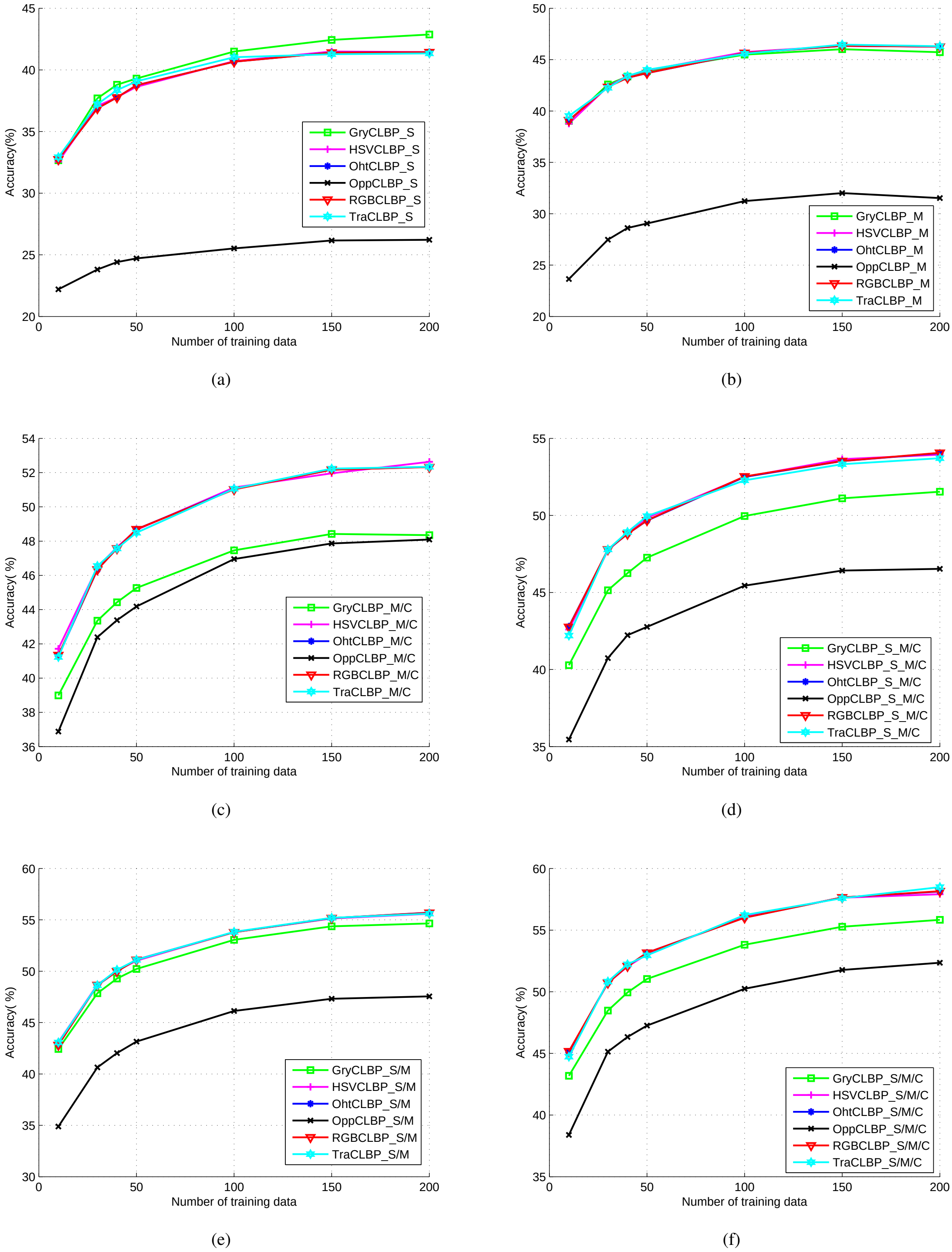

Fig. 7. Recognition accuracy as a function of the number of training images for OT8 image dataset using the gray CLBP descriptors and the proposed CCLBP descriptors when R=1 and P=8. 7(a) CLBP_S and CCLBP_S. 7(b) CLBP_M and CCLBP_M. 7(c) CLBP_M/C and CCLBP_M/C. 7(d) CLBP_S_M/C and CCLBP_S_M/C. 7(e) CLBP_S/M and CCLBP_S/M. 7(f) CLBP_S/M/C and CCLBP_S/M/C.

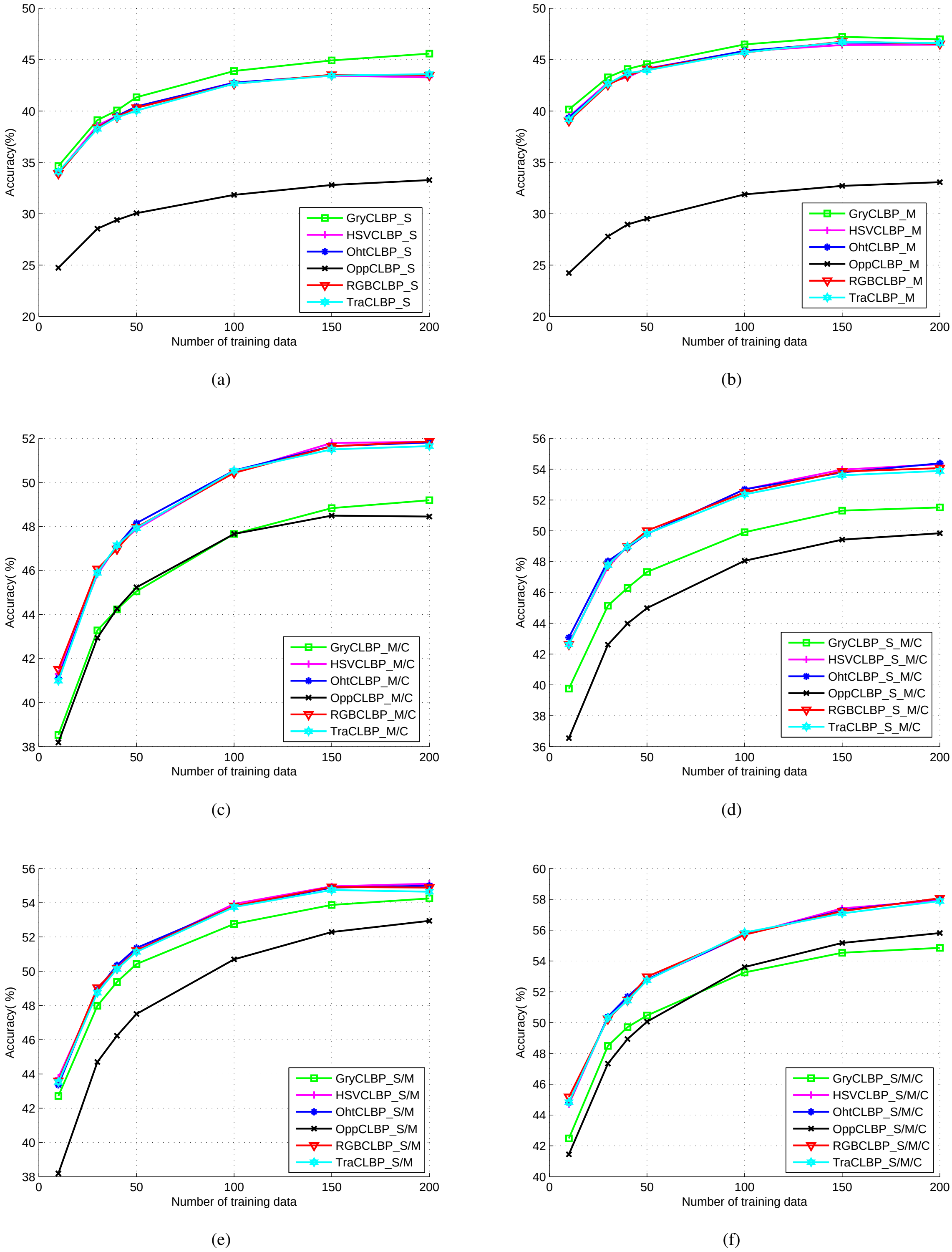

Fig. 8. Recognition accuracy as a function of the number of training images for OT8 image dataset using the gray CLBP descriptors and the proposed CCLBP descriptors when R=2 and P=16. 8(a) CLBP_S and CCLBP_S. 8(b) CLBP_M and CCLBP_M. 8(c) CLBP_M/C and CCLBP_M/C. 8(d) CLBP_S_M/C and CCLBP_S_M/C. 8(e) CLBP_S/M and CCLBP_S/M. 8(f) CLBP_S/M/C and CCLBP_S/M/C.

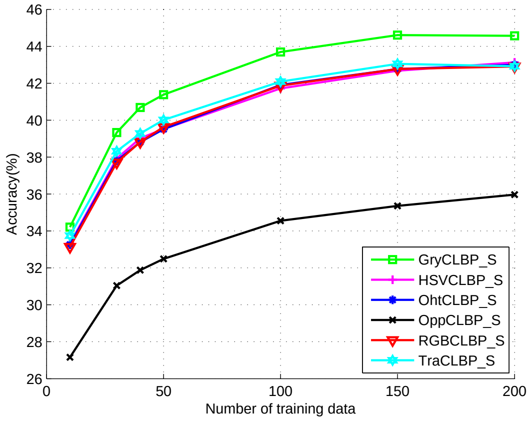

(a)

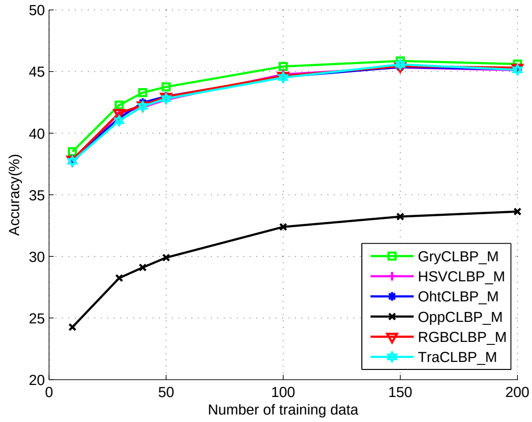

(b)

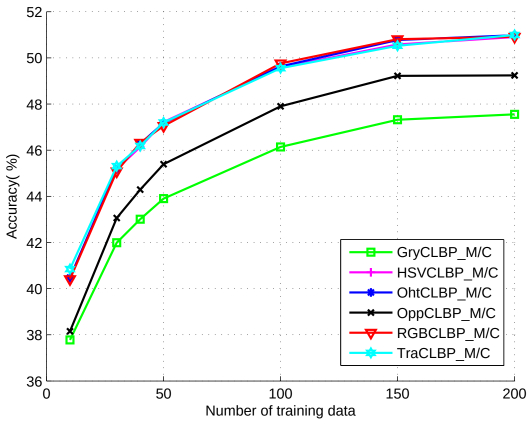

(c)

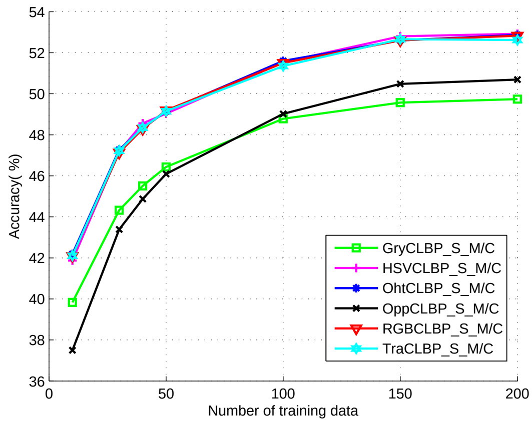

(d)

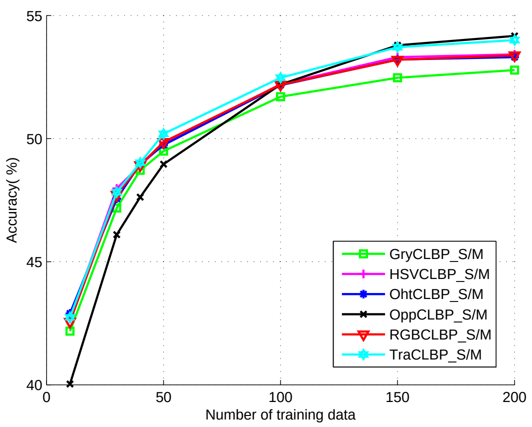

(e)

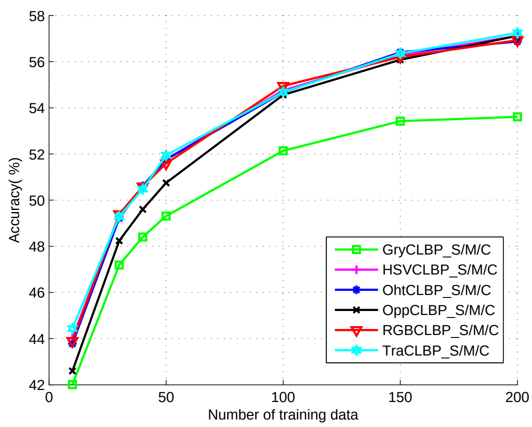

(f)

Fig. 9. Recognition accuracy as a function of the number of training images for OT8 image dataset using the gray CLBP descriptors and the proposed CCLBP descriptors when R=3 and P=24. 9(a) CLBP_S and CCLBP_S. 9(b) CLBP_M and CCLBP_M. 9(c) CLBP_M/C and CCLBP_M/C. 9(d) CLBP_S_M/C and CCLBP_S_M/C. 9(e) CLBP_S/M and CCLBP_S/M. 9(f) CLBP_S/M/C and CCLBP_S/M/C.

TABLE I
CLASSIFICATION RATES (%) ON OT8 DATABASE

	R=1,P=8							R=2,P=16							R=3,P=24						
	10	***30***	***40***	***50***	***100***	***150***	***200***	***10***	***30***	***40***	***50***	***100***	***150***	***200***	***10***	***30***	***40***	***50***	***100***	***150***	***200***
Gray_CLBP_S	32.67	37.69	38.80	39.30	41.49	42.43	**42.87**	34.64	39.11	40.05	41.34	43.89	44.92	**45.58**	34.21	39.33	40.69	41.38	43.69	**44.61**	44.57
HSV_CLBP_S	32.56	37.07	37.78	38.63	40.71	41.49	41.44	34.01	38.58	39.53	40.43	42.77	43.43	43.28	33.32	37.92	39.02	39.52	41.72	42.68	43.13
OHTA_CLBP_S	32.75	36.88	37.77	38.76	40.66	41.41	41.44	33.92	38.37	39.51	40.44	42.75	43.47	43.48	33.26	37.80	38.81	39.51	41.91	42.77	43.00
OPP_CLBP_S	22.20	23.81	24.41	24.71	25.52	26.16	26.22	24.74	28.54	29.39	30.05	31.84	32.80	33.28	27.16	31.04	31.88	32.49	34.55	35.36	35.97
RGB_CLBP_S	32.74	36.88	37.77	38.75	40.66	41.40	41.43	33.91	38.36	39.41	40.32	42.64	43.53	43.48	33.14	37.71	38.82	39.63	41.87	42.77	42.91
TRANS_CLBP_S	32.92	37.22	38.36	39.07	41.03	41.27	41.34	34.09	38.26	39.37	40.03	42.66	43.44	43.59	33.75	38.32	39.28	40.01	42.09	43.05	42.92
Gray_CLBP_M	39.03	42.59	43.35	43.87	45.49	46.01	45.72	40.15	43.28	44.08	44.56	46.48	47.22	46.98	38.50	42.27	43.29	43.75	45.41	**45.86**	45.60
HSV_CLBP_M	38.77	42.38	43.40	43.95	45.73	46.34	46.26	39.45	42.77	43.28	44.14	45.81	46.42	46.45	37.60	41.62	42.10	42.71	44.77	45.33	45.11
OHTA_CLBP_M	39.10	42.37	43.23	43.69	45.63	46.33	46.28	39.37	42.61	43.45	44.09	45.85	46.66	46.59	37.87	41.22	42.48	42.98	44.56	45.36	45.18
OPP_CLBP_M	23.65	27.47	28.61	29.05	31.23	32.01	31.52	24.23	27.79	28.95	29.52	31.88	32.71	33.07	24.26	28.24	29.10	29.90	32.39	33.23	33.64
RGB_CLBP_M	39.10	42.33	43.24	43.69	45.65	46.34	46.27	39.04	42.56	43.43	44.08	45.68	46.75	46.53	37.85	41.64	42.25	42.96	44.65	45.43	45.31
TRANS_CLBP_M	39.52	42.25	43.40	44.01	45.57	**46.46**	46.30	39.18	42.65	43.68	43.96	45.70	46.71	46.62	37.72	41.01	42.17	42.80	44.51	45.57	45.14
Gray_CLBP_M/C	38.99	43.35	44.43	45.26	47.46	48.42	48.35	38.53	43.28	44.23	45.05	47.66	48.83	49.19	37.78	41.99	43.01	43.90	46.14	47.32	47.55
HSV_CLBP_M/C	41.71	46.48	47.64	48.66	51.13	51.96	**52.63**	41.30	45.82	47.12	47.87	50.47	51.79	51.85	40.45	45.18	46.14	**47.22**	49.58	50.58	50.90
OHTA_CLBP_M/C	41.29	46.33	47.57	48.69	51.04	52.17	52.33	41.12	45.90	47.11	48.15	50.54	51.65	51.81	40.48	45.17	46.28	47.18	49.63	50.77	50.98
OPP_CLBP_M/C	36.88	42.39	43.38	44.18	46.95	47.86	48.09	38.19	42.94	44.26	45.23	47.66	48.49	48.45	38.15	43.06	44.29	45.39	47.90	49.22	49.24
RGB_CLBP_M/C	41.34	46.34	47.57	48.69	51.02	52.17	52.32	41.51	46.07	46.97	47.96	50.43	51.64	**51.86**	40.41	45.08	46.32	47.05	49.76	50.81	50.91
TRANS_CLBP_M/C	41.23	46.55	47.57	48.49	51.06	52.23	52.34	40.99	45.89	47.15	47.92	50.53	51.50	51.65	40.85	45.31	46.18	47.20	49.55	50.52	**50.99**
Gray_CLBP_S_M/C	40.28	45.14	46.25	47.26	49.96	51.11	51.54	39.76	45.14	46.29	47.33	49.91	51.31	51.52	39.83	44.32	45.51	46.43	48.78	49.57	49.74
HSV_CLBP_S_M/C	42.59	47.73	48.89	49.85	52.50	53.65	53.94	42.71	47.65	48.99	49.80	52.69	53.97	54.32	41.87	47.19	48.56	49.03	51.54	52.80	**52.92**
OHTA_CLBP_S_M/C	42.79	47.77	48.80	49.66	52.50	53.52	54.04	43.08	48.03	48.90	49.80	52.69	53.79	**54.38**	42.19	47.27	48.32	49.15	51.60	52.60	52.87
OPP_CLBP_S_M/C	35.46	40.74	42.23	42.77	45.44	46.42	46.53	36.55	42.61	43.98	44.99	48.06	49.43	49.84	37.50	43.39	44.87	46.09	49.02	50.48	50.69
RGB_CLBP_S_M/C	42.76	47.79	48.80	49.68	52.53	53.53	**54.06**	42.63	47.78	48.98	50.01	52.49	53.85	54.07	42.09	47.13	48.29	49.19	51.50	52.60	52.83
TRANS_CLBP_S_M/C	42.20	47.79	48.92	49.95	52.28	53.32	53.71	42.62	47.78	48.98	49.81	52.36	53.60	53.89	42.10	47.22	48.35	49.15	51.35	52.66	52.62
Gray_CLBP_S/M	42.43	47.85	49.28	50.22	53.05	54.37	54.65	42.71	47.98	49.37	50.42	52.76	53.87	54.25	42.18	47.18	48.71	49.49	51.70	52.47	52.78
HSV_CLBP_S/M	43.10	48.68	50.04	51.03	53.80	55.14	55.58	43.78	48.88	50.32	51.22	53.93	54.96	**55.11**	42.68	47.97	48.91	49.79	52.21	53.31	53.42
OHTA_CLBP_S/M	42.86	48.63	50.00	51.12	53.80	55.17	**55.70**	43.36	48.92	50.35	51.36	53.79	54.88	54.99	42.90	47.56	48.97	49.74	52.17	53.21	53.31
OPP_CLBP_S/M	34.88	40.64	42.03	43.15	46.13	47.32	47.55	38.19	44.70	46.23	47.50	50.69	52.29	52.94	40.03	46.10	47.62	48.96	52.20	53.79	**54.17**
RGB_CLBP_S/M	42.81	48.65	49.99	51.11	53.79	55.18	55.68	43.59	49.04	50.18	51.20	53.81	54.92	54.88	42.56	47.72	48.92	49.86	52.19	53.20	53.38
TRANS_CLBP_S/M	43.06	48.63	50.13	51.11	53.83	55.19	55.60	43.53	48.74	50.13	51.13	53.75	54.74	54.64	42.74	47.82	49.02	50.19	52.47	53.71	54.00
Gray_CLBP_S/M/C	43.18	48.47	49.94	51.04	53.81	55.27	55.83	42.48	48.49	49.70	50.46	53.25	54.53	54.85	42.01	47.19	48.40	49.31	52.14	53.42	53.61
HSV_CLBP_S/M/C	45.15	50.71	52.04	53.03	56.12	57.63	57.91	44.70	50.35	51.54	52.79	55.69	57.41	57.93	44.03	49.29	50.57	51.77	54.75	56.27	57.12
OHTA_CLBP_S/M/C	45.11	50.74	52.08	53.16	56.01	57.65	58.13	44.80	50.38	51.68	52.80	55.72	57.28	58.05	43.78	49.21	50.62	51.76	54.67	56.41	56.87
OPP_CLBP_S/M/C	38.39	45.14	46.33	47.26	50.24	51.77	52.35	41.45	47.34	48.93	50.06	53.60	55.17	55.81	42.60	48.24	49.60	50.75	54.56	56.08	57.12
RGB_CLBP_S/M/C	45.17	50.72	52.08	53.16	56.00	57.65	58.15	45.18	50.24	51.46	52.97	55.70	57.23	**58.07**	43.90	49.39	50.59	51.59	54.95	56.20	56.93
TRANS_CLBP_S/M/C	44.73	50.83	52.22	52.95	56.22	57.59	**58.49**	44.83	50.31	51.42	52.74	55.84	57.08	57.89	44.44	49.29	50.48	51.95	54.68	56.35	**57.25**

Opponent $CCLBP\_M/C$ operator has outperformed the gray $CLBP\_M/C$ and remaining $CCLBP\_M/C$ operators. Thirdly, the gray $CLBP\_M/C$ and $CLBP\_S/M/C$ operators have performed worse than all $CCLBP\_M/C$ and $CCLBP\_S/M/C$ operators, respectively. Lastly, the performances of the gray $CLBP\_S\_M/C$ and the Opponent $CCLBP\_S\_M/C$ operators are approximately the same and have performed worse than the remaining $CCLBP\_S\_M/C$ operators. The Transformed $CCLBP\_S/M/C$ operator has achieved the best classification accuracy, which reached up 52.11%, while the gray $CLBP\_S\_M/C$ operator has achieved 48.86% classification accuracy.

Figs. 11(a) to 11(f) show the performances of the texture operators of the $R = 2$ and $P = 16$ texture pattern. The following observations can be obtained from these figures. Firstly, the gray CLBP_M operator has outperformed all $CCLBP\_M$ operators, while the remaining gray CLBP operators have performed worse than the other CCLBP operators, except for the gray $CLBP\_S$ that has performed better than the Opponent $CCLBP\_S$ operator. Secondly, aside from the Opponent $CCLBP\_S$ and Opponent $CCLBP\_M$ operators, the remaining Opponent CCLBP operators have outperformed the gray CLBP and the other CCLBP operators. Finally, the Opponent $CCLBP\_S/M/C$ operator has achieved the best classification accuracy, which has reached up to 53.54%, and is closely followed by the Transformed $CCLBP\_S/M/C$, which has achieved a 52.84% classification accuracy.

Figs. 12(a) to 12(f) demonstrate the performances of the texture operators of the $R = 3$ and $P = 24$ texture pattern. The following observations can be obtained from these figures. Firstly, the responses of the CLBP operators are nearly similar to their responses of the $R = 2$ and $P = 16$ texture pattern, except for the Opponent $CCLBP\_S\_M/C$ and Opponent $CCLBP\_S/M$ operators, which have outperformed the other CLBP operators. Secondly, only the gray $CLBP\_M$ has outperformed the $CCLBP\_M$ operators while the remaining CCLBP operators have outperformed the remaining gray CLBP operators. Lastly, the Opponent $CCLBP\_S/M/C$ operator has achieved the best classification accuracy, which has reached up to 55.05%, and is followed by the Transformed $CCLBP\_S/M/C$ at 52.49% classification accuracy. Table II shows the classification accuracy results on Event database in details. Generally speaking, the CCLBP operators have outperformed the gray CLBP operators.

Overall, the $CCLBP\_S/M/C$ operators have achieved the best classification accuracy in both OT8 and Event Sport experiments. Table III summarizes the $CCLBP\_S/M/C$ operators results. In OT8 experiments, The best classification accuracy that is achieved using the gray CLBP operators is 55.83% by $CLBP\_S/M/C_{1,8}$, and 58.49% by Transformed $CCLBP\_S/M/C_{1,8}$. On the other hand, the Opponent $CCLBP\_S/M/C_{3,24}$ has achieved the best classification accuracy in Event Sport experiments, which reached up 55.05%, while the best classification accuracy that is achieved using the gray CLBP operators is 49.85% by $CLBP\_S/M/C_{2,16}$.

VI. CONCLUSION

This paper incorporated the Completed Local Binary Pattern (CLBP) with different colour information to enhance its photometric invariance and its discriminating property. Five novel multi-scale colour CLBP (CCLBP) texture descriptors were proposed and evaluated for image categorisation. OT8 and Event sport datasets were used to evaluate the proposed CCLBP and to compare it with the gray CLBP. The results attested to the superiority of the proposed CCLBP over the original gray CLBP.

VII. FUTURE WORK

In the future work, the late fusion features strategy will be used to combine all the proposed colour CCLBP (CCLBP). In addition, the proposed CCLBP will combined with different descriptors such as SIFT, and CLTP.

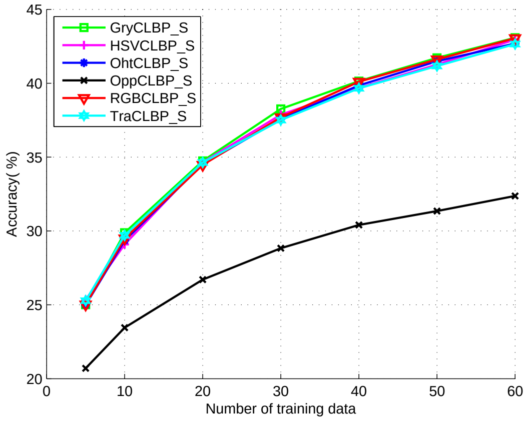

(a)

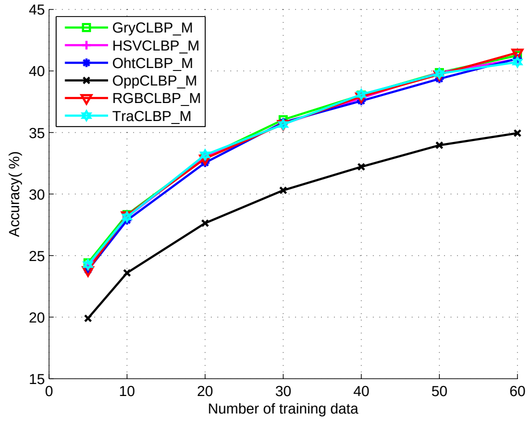

(b)

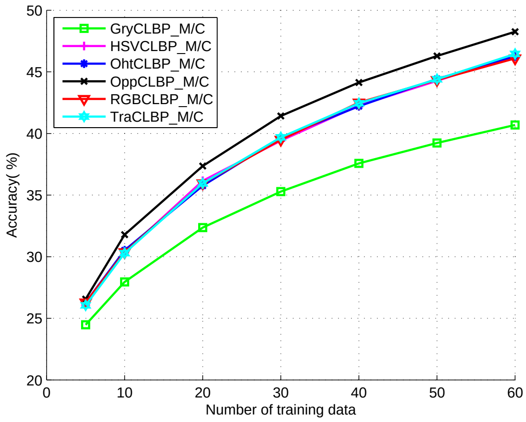

(c)

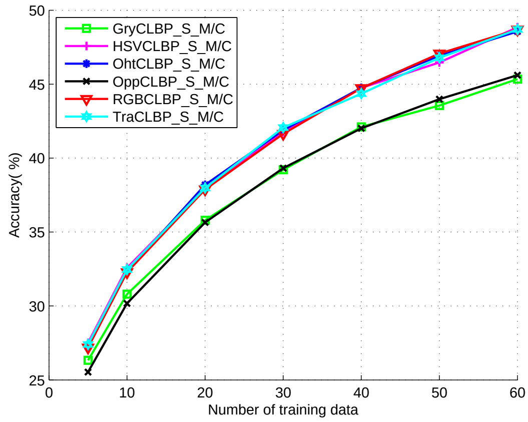

(d)

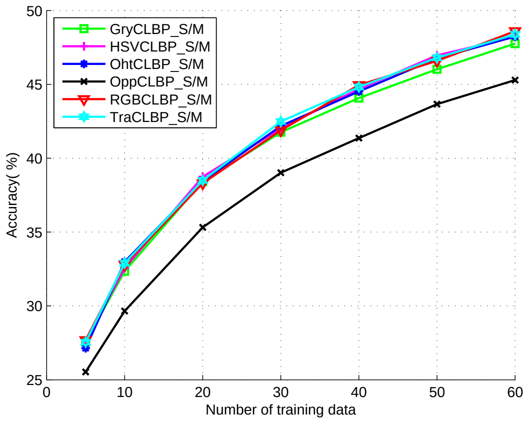

(e)

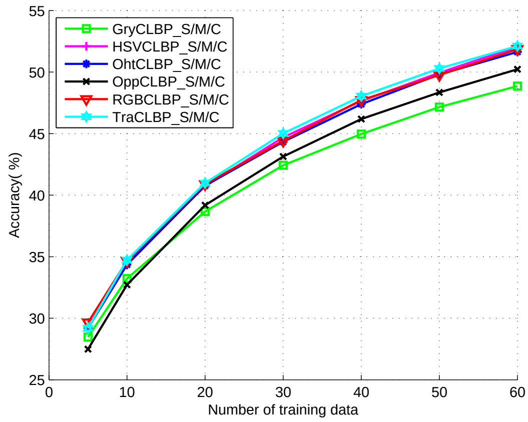

(f)

Fig. 10. Recognition accuracy as a function of the number of training images for Event sport image dataset using the gray CLBP descriptors and the proposed CCLBP descriptors when R=1 and P=8 10(a) CLBP_S and CCLBP_S. 10(b) CLBP_M and CCLBP_M. 10(c) CLBP_M/C and CCLBP_M/C. 10(d) CLBP_S_M/C and CCLBP_S_M/C. 10(e) CLBP_S/M and CCLBP_S/M. 10(f) CLBP_S/M/C and CCLBP_S/M/C.

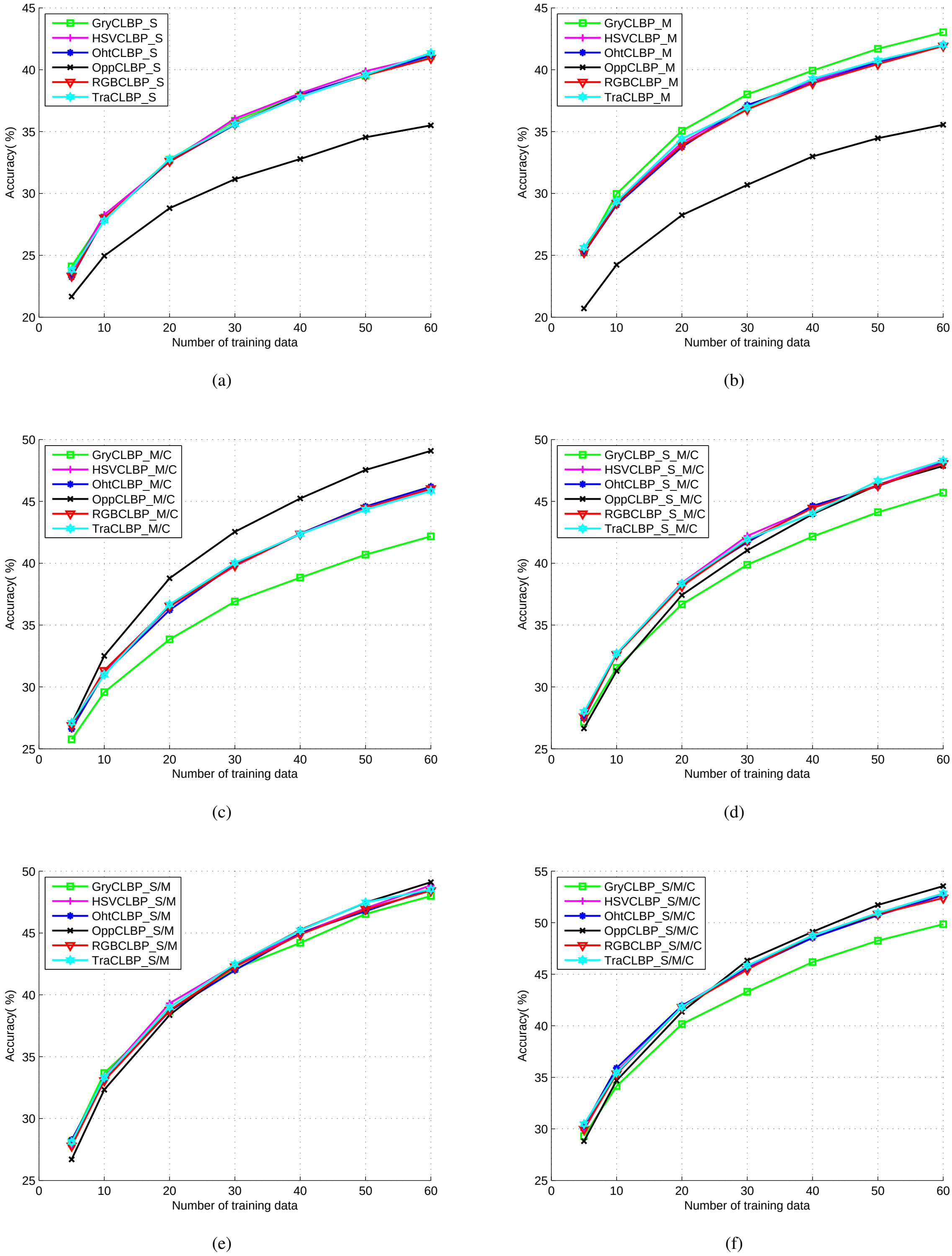

Fig. 11. Recognition accuracy as a function of the number of training images for Event sport image dataset using the gray CLBP descriptors and the proposed CCLBP descriptors when R=2 and P=16. 8(a) CLBP_S and CCLBP_S. 11(b) CLBP_M and CCLBP_M. 11(c) CLBP_M/C and CCLBP_M/C. 11(d) CLBP_S_M/C and CCLBP_S_M/C. 8(e) CLBP_S/M and CCLBP_S/M. 11(f) CLBP_S/M/C and CCLBP_S/M/C.

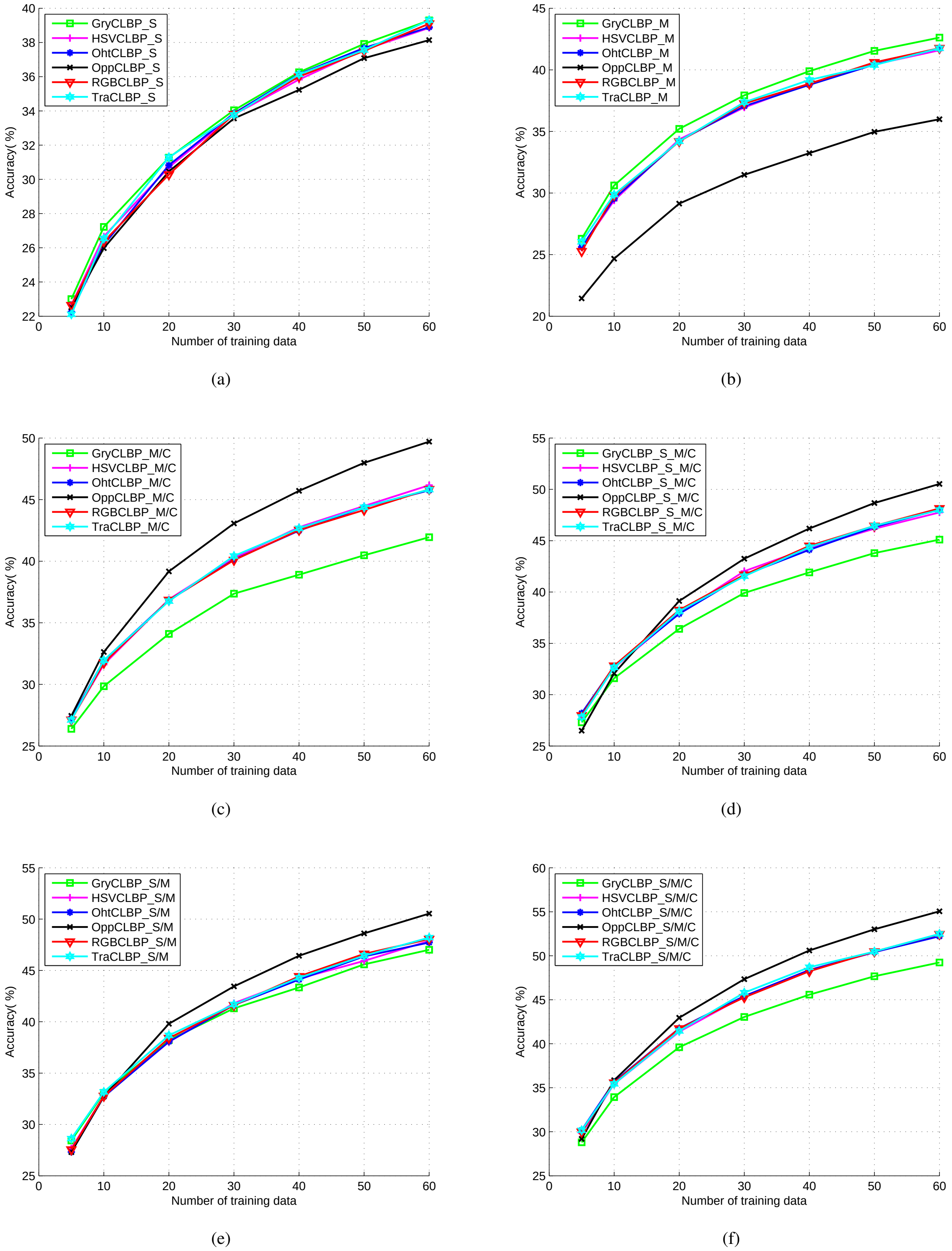

Fig. 12. Recognition accuracy as a function of the number of training images for Event sport image dataset using the gray CLBP descriptors and the proposed CCLBP descriptors when R=3 and P=24. 12(a) CLBP_S and CCLBP_S. 12(b) CLBP_M and CCLBP_M. 12(c) CLBP_M/C and CCLBP_M/C. 12(d) CLBP_S_M/C and CCLBP_S_M/C. 12(e) CLBP_S/M and CCLBP_S/M. 12(f) CLBP_S/M/C and CCLBP_S/M/C.

TABLE II
CLASSIFICATION RATES (%) ON EVENT DATABASE

	R=1,P=8							R=2,P=16							R=3,P=24						
	5	*10*	*20*	*30*	*40*	*50*	*60*	*5*	*10*	*20*	*30*	*40*	*50*	*60*	*5*	*10*	*20*	*30*	*40*	*50*	*60*
Gray_CLBP_S	25.01	29.88	34.74	38.26	40.14	41.72	**43.08**	24.11	28.07	32.73	35.88	37.98	39.51	41.09	23.00	27.22	31.27	34.04	36.26	37.92	39.29
HSV_CLBP_S	25.34	29.09	34.65	37.87	39.68	41.26	42.96	23.64	28.28	32.60	36.05	38.10	39.89	41.14	22.66	26.66	30.71	33.79	35.83	37.58	38.85
OHTA_CLBP_S	24.99	29.35	34.51	37.58	39.85	41.49	42.69	23.24	27.97	32.57	35.57	37.97	39.59	41.15	22.26	26.18	30.83	33.86	36.15	37.68	38.89
OPP_CLBP_S	20.70	23.45	26.71	28.83	30.41	31.35	32.37	21.67	24.95	28.81	31.15	32.78	34.54	35.50	22.53	25.98	30.46	33.56	35.23	37.08	38.14
RGB_CLBP_S	25.02	29.49	34.47	37.69	40.10	41.61	43.05	23.32	28.02	32.61	35.62	37.85	39.54	40.94	22.64	26.37	30.28	33.81	36.00	37.51	39.10
TRANS_CLBP_S	25.28	29.70	34.63	37.51	39.66	41.17	42.65	23.82	27.82	32.79	35.61	37.80	39.59	**41.36**	22.11	26.54	31.29	33.77	36.13	37.56	**39.30**
Gray_CLBP_M	24.41	28.33	33.00	36.04	38.03	39.86	41.26	25.23	29.97	35.07	38.01	39.93	41.69	**43.03**	26.29	30.62	35.21	37.93	39.89	41.54	**42.62**
HSV_CLBP_M	24.06	28.12	33.05	35.70	37.80	39.86	40.95	25.16	29.32	34.10	37.08	39.11	40.70	42.02	25.60	29.39	34.35	36.95	38.89	40.44	41.59
OHTA_CLBP_M	23.83	27.87	32.54	35.82	37.57	39.36	41.00	25.19	29.06	33.75	37.14	38.94	40.62	42.02	25.62	29.54	34.23	37.05	38.78	40.43	41.74
OPP_CLBP_M	19.90	23.59	27.63	30.30	32.21	33.96	34.95	20.71	24.23	28.25	30.69	32.99	34.46	35.55	21.45	24.67	29.14	31.48	33.24	34.97	35.99
RGB_CLBP_M	23.82	28.28	32.88	35.70	37.93	39.72	**41.49**	25.24	29.21	33.91	36.79	38.91	40.46	41.92	25.27	29.81	34.19	37.26	38.87	40.61	41.76
TRANS_CLBP_M	24.26	28.14	33.18	35.65	38.09	39.79	40.72	25.62	29.36	34.42	36.95	39.27	40.75	42.01	26.04	29.88	34.20	37.37	39.18	40.39	41.75
Gray_CLBP_M/C	24.47	27.95	32.36	35.28	37.57	39.23	40.69	25.77	29.58	33.85	36.91	38.84	40.70	42.17	26.39	29.85	34.10	37.36	38.90	40.48	41.95
HSV_CLBP_M/C	26.07	30.35	36.16	39.41	42.26	44.27	46.32	26.99	31.23	36.49	39.78	42.37	44.33	46.00	27.17	31.62	36.90	40.26	42.76	44.48	46.17
OHTA_CLBP_M/C	26.29	30.52	35.76	39.65	42.21	44.43	46.24	26.60	31.10	36.21	39.91	42.39	44.59	46.19	27.24	31.94	36.83	40.13	42.48	44.38	45.75
OPP_CLBP_M/C	26.56	31.79	37.36	41.42	44.13	46.29	**48.25**	27.03	32.51	38.78	42.54	45.23	47.54	**49.08**	27.45	32.63	39.17	43.07	45.71	47.98	**49.70**
RGB_CLBP_M/C	26.29	30.37	35.95	39.49	42.51	44.34	46.09	26.89	31.34	36.54	39.81	42.36	44.46	46.04	27.12	31.74	36.85	40.09	42.53	44.15	45.84
TRANS_CLBP_M/C	26.05	30.29	35.95	39.68	42.45	44.40	46.45	27.11	30.99	36.67	40.03	42.36	44.34	45.85	27.11	31.96	36.76	40.42	42.67	44.38	45.82
Gray_CLBP_S_M/C	26.33	30.80	35.80	39.21	42.11	43.55	45.34	27.16	31.55	36.68	39.88	42.16	44.12	45.70	27.30	31.60	36.41	39.90	41.91	43.79	45.10
HSV_CLBP_S_M/C	27.50	32.58	37.95	41.76	44.75	46.47	**48.84**	27.79	32.67	38.42	42.21	44.46	46.31	48.23	27.95	32.63	37.94	42.03	44.29	46.16	47.75
OHTA_CLBP_S_M/C	27.24	32.34	38.19	41.89	44.75	46.92	48.56	27.47	32.70	38.35	41.69	44.63	46.23	48.12	28.19	32.76	37.88	41.66	44.11	46.33	48.02
OPP_CLBP_S_M/C	25.53	30.17	35.65	39.32	42.01	43.98	45.61	26.65	31.29	37.43	41.04	43.97	46.33	47.86	26.49	32.07	39.12	43.24	46.18	48.67	**50.53**
RGB_CLBP_S_M/C	27.19	32.28	37.88	41.64	44.73	47.07	48.69	27.59	32.62	38.14	41.85	44.46	46.28	48.06	27.97	32.81	38.24	41.67	44.49	46.44	48.14
TRANS_CLBP_S_M/C	27.40	32.46	37.98	42.06	44.36	46.78	48.70	27.99	32.72	38.36	41.93	44.04	46.67	**48.30**	27.83	32.66	38.12	41.54	44.37	46.45	47.98
Gray_CLBP_S/M	27.56	32.35	38.42	41.76	44.07	46.02	47.76	28.14	33.69	38.65	42.11	44.20	46.54	47.99	28.43	33.08	38.22	41.30	43.34	45.59	47.01
HSV_CLBP_S/M	27.62	32.55	38.74	42.03	44.68	46.96	48.21	27.75	33.35	39.32	42.42	44.97	47.00	48.85	27.66	32.77	38.03	41.81	44.21	45.93	47.88
OHTA_CLBP_S/M	27.14	32.99	38.44	42.18	44.52	46.76	48.24	28.28	33.10	38.69	41.99	44.99	46.76	48.56	27.31	32.71	38.06	41.63	44.11	46.37	47.72
OPP_CLBP_S/M	25.53	29.65	35.32	39.02	41.36	43.66	45.29	26.70	32.33	38.37	42.44	45.25	47.46	**49.10**	27.30	32.73	39.81	43.45	46.43	48.61	**50.54**
RGB_CLBP_S/M	27.68	32.79	38.30	41.89	44.95	46.59	**48.60**	27.79	33.07	38.75	42.27	44.88	46.93	48.42	27.55	32.77	38.40	41.61	44.42	46.61	48.05
TRANS_CLBP_S/M	27.54	32.90	38.50	42.48	44.82	46.80	48.38	28.10	33.32	39.00	42.48	45.22	47.48	48.53	28.62	33.16	38.68	41.68	44.28	46.44	48.20
Gray_CLBP_S/M/C	28.47	33.22	38.67	42.42	44.97	47.16	48.86	29.30	34.15	40.17	43.31	46.17	48.26	49.85	28.80	33.94	39.60	43.04	45.58	47.67	49.24
HSV_CLBP_S/M/C	29.27	34.58	40.73	44.69	47.65	49.94	52.06	29.87	35.55	41.92	45.74	48.53	50.75	52.68	29.85	35.43	41.37	45.38	48.38	50.39	52.39
OHTA_CLBP_S/M/C	29.20	34.35	40.77	44.33	47.39	49.81	51.64	30.26	35.90	41.95	45.55	48.53	50.71	52.68	30.19	35.67	41.75	45.42	48.37	50.42	52.21
OPP_CLBP_S/M/C	27.49	32.72	39.18	43.14	46.18	48.34	50.22	28.81	34.68	41.35	46.33	49.11	51.71	**53.54**	29.19	35.85	42.95	47.34	50.60	53.01	**55.05**
RGB_CLBP_S/M/C	29.66	34.65	40.90	44.41	47.72	49.76	51.87	29.97	35.35	41.80	45.45	48.78	50.83	52.40	29.99	35.57	41.73	45.27	48.24	50.47	52.45
TRANS_CLBP_S/M/C	29.19	34.73	40.98	45.01	48.04	50.29	**52.11**	30.47	35.45	41.82	45.83	48.75	50.94	52.84	30.16	35.45	41.45	45.81	48.69	50.47	52.49

TABLE III
THE GRAY CLBP AND CCLBP_S/M/C OPERATORS CLASSIFICATION ACCURACY RESULTS

Descriptor	Dataset	P=8,R=1	P=16,R=2	P=24,R=3
Gray_CLBP_S/M/C	OT8	55.83	54.85	53.61
HSV_CLBP_S/M/C		57.91	57.93	57.12
OHTA_CLBP_S/M/C		58.13	58.05	56.87
OPP_CLBP_S/M/C		52.35	55.81	57.12
RGB_CLBP_S/M/C		58.15	58.07	56.93
TRANS_CLBP_S/M/C		**58.49**	57.89	57.25
Gray_CLBP_S/M/C	Event Sport	48.86	49.85	49.24
HSV_CLBP_S/M/C		52.06	52.68	52.39
OHTA_CLBP_S/M/C		51.64	52.68	52.21
OPP_CLBP_S/M/C		50.22	53.54	**55.05**
RGB_CLBP_S/M/C		51.87	52.40	52.45
TRANS_CLBP_S/M/C		52.11	52.84	52.49

ACKNOWLEDGMENT

The authors would like to thank the anonymous reviewers for their helpful comments and suggestions. This work is supported by the Universiti Malaysia Pahang (UMP) via Research Grant UMP RDU160349.

REFERENCES

[1] X. Wang, T. Han, and S. Yan, "An HOG-LBP human detector with partial occlusion handling," in *Proceedings of 12th IEEE International Conference of Computer Vision*, 2009, pp. 32–39.

[2] A. A. Fathima, S. Vasuhi, N. N. Babu, V. Vaidehi, and T. M. Treesa, "Fusion framework for multimodal biometric person authentication system," *IAENG International Journal of Computer Science*, vol. 41, no. 1, pp. 18–31, 2014.

[3] T. H. Rassem, N. M. Makbol, and S. Y. Yee, "Face recognition using completed local ternary pattern (CLTP) texture descriptor," *International Journal of Electrical and Computer Engineering*, vol. 7, no. 3, 2017.

[4] M.-H. Tsai, Y.-K. Chan, J.-S. Wang, S.-W. Guo, and J.-L. Wu, "Color-texture-based image retrieval system using gaussian markov random field model," *Mathematical Problems in Engineering*, vol. 2009, Article ID 410243, 17 pages, 2009.

[5] S. Murala, R. P. Maheshwari, and R. Balasubramanian, "Local tetra patterns: A new feature descriptor for content-based image retrieval," *IEEE Transactions on Image Processing*, vol. 21, no. 5, pp. 2874–2886, May 2012.

[6] Z. Xia, C. Yuan, X. Sun, D. Sun, and R. Lv, "Combining wavelet transform and LBP related features for fingerprint liveness detection," *IAENG International Journal of Computer Science*, vol. 43, no. 3, pp. 290–298, 2016.

[7] B.-Y. Park, H.-H. Kim, and B.-W. Hong, "A multilabel texture segmentation based on local entropy signature," *Mathematical Problems in Engineering*, vol. 2013, Article ID 651581, 6 pages, 2013.

[8] J. Xiao, J. Hays, K. Ehinger, A. Oliva, and A. Torralba, "SUN database: Large-scale scene recognition from abbey to zoo," in *Proceedings of the 2010 IEEE Computer Society Conference on Computer Vision and Pattern Recognition*, 2010, pp. 3485 –3492.

[9] T. H. Rassem, M. F. Mohammed, B. E. Khoo, and N. M. Makbol, "Performance evaluation of completed local ternary patterns (CLTP) for medical, scene and event image categorisation," in *Software Engineering and Computer Systems (ICSECS), 2015 4th International Conference on*. IEEE, 2015, pp. 33–38.

[10] I. K. E. P. M. H. Ingrid Nurtanio, Eha Renwi Astuti and M. H. Purnomo, "Classifying cyst and tumor lesion using support vector machine based on dental panoramic images texture features," *IAENG International Journal of Computer Science*, vol. 40, no. 1, pp. 29–37, 2013.

[11] J. Zhang and T. Tan, "Brief review of invariant texture analysis methods," *Pattern Recognition*, vol. 35, no. 3, pp. 735 – 747, 2002.

[12] T. Reed and J. Dubuf, "A review of recent texture segmentation and feature extraction techniques," *CVGIP: Image Understanding*, vol. 57, no. 3, pp. 359 – 372, 1993.

[13] T. Ojala, M. Pietikinen, and D. Harwood, "A comparative study of texture measures with classification based on featured distributions," *Pattern Recognition*, vol. 29, no. 1, pp. 51 – 59, 1996.

[14] T. Ojala, M. Pietikainen, and T. Maenpaa, "Multiresolution gray-scale and rotation invariant texture classification with local binary patterns," *IEEE Transactions on Pattern Analysis and Machine Intelligence*, vol. 24, no. 7, pp. 971–987, July 2002.

[15] J.-Y. Choi, Y.-M. Ro, and K. Plataniotis, "Color local texture features for color face recognition," *IEEE Transactions on Image Processing*, vol. 21, no. 3, pp. 1366–1380, 2012.

[16] M. Heikkil, M. Pietikinen, and C. Schmid, "Description of interest regions with center-symmetric local binary patterns," in *Proceedings of 5th Indian Conference of Computer Vision, Graphics and Image Processing*, 2006, vol. 4338, pp. 58–69.

[17] S. Liao, M. Law, and A. Chung, "Dominant local binary patterns for texture classification," *IEEE Transactions on Image Processing*, vol. 18, no. 5, pp. 1107–1118, May 2009.

[18] X. Tan and B. Triggs, "Enhanced local texture feature sets for face recognition under difficult lighting conditions," *IEEE Transactions on Pattern Analysis and Machine Intelligence*, vol. 19, no. 6, pp. 1635–1650, June 2010.

[19] Z. Guo, L. Zhang, and D. Zhang, "A completed modeling of local binary pattern operator for texture classification," *IEEE Transactions on Image Processing*, vol. 19, no. 6, pp. 1657–1663, Jun 2010.

[20] T. H. Rassem and B. E. Khoo, "Completed local ternary pattern for rotation invariant texture classification," *The Scientific World Journal*, vol. (2014), , 10 pages.
[21] X. Qi, G. Zhao, L. Shen, Q. Li, and M. Pietikinen, "Load: Local orientation adaptive descriptor for texture and material classification," *Neurocomputing*, vol. 184, pp. 28 – 35, 2016.
[22] C. Zhu, C.-E. Bichot, and L. Chen, "Multi-scale color local binary patterns for visual object classes recognition," in *Proceedings of 20th International Conference on Pattern Recognition*, 2010, pp. 3065–3068.
[23] S. Banerji, A. Verma, and C. Liu, "Novel color LBP descriptors for scene and image texture classification," in *Proceedings of 15th International Conference on Image Processing, Computer Vision, and Pattern Recognition*, 2011, pp. 537–543.
[24] N. Dalal and B. Triggs, "Histograms of oriented gradients for human detection," in *Proceedings of the 2005 IEEE Conference on Computer Vision and Pattern Recognition*, 2005, pp. 886–893.
[25] A. Abdel-Hakim and A. Farag, "CSIFT: A sift descriptor with color invariant characteristics," in *Proceedings of the 2006 IEEE Computer Society Conference on Computer Vision and Pattern Recognition*, 2006, pp. 1978 – 1983.
[26] K. van de Sande, T. Gevers, and C. Snoek, "Evaluating color descriptors for object and scene recognition," *IEEE Transactions on Pattern Analysis and Machine Intelligence*, vol. 32, no. 9, pp. 1582 –1596, 2010.
[27] A. Gijsenij, T. Gevers, and J. Van De Weijer, "Improving color constancy by photometric edge weighting," *IEEE Transactions on Pattern Analysis and Machine Intelligence,*, vol. 34, no. 5, pp. 918–929, 2012.
[28] J. Van De Weijer, T. Gevers, and A. D. Bagdanov, "Boosting color saliency in image feature detection," *Pattern Analysis and Machine Intelligence, IEEE Transactions on*, vol. 28, no. 1, pp. 150–156, 2006.
[29] C. G. Snoek, K. E. van de Sande, X. Li, M. Mazloom, Y.-G. Jiang, D. C. Koelma, and A. W. Smeulders, "The mediamill TRECVID 2011 semantic video search engine," in *Proceedings of the 9th TRECVID Workshop*, 2011.
[30] Y.-I. Ohta, T. Kanade, and T. Sakai, "Color information for region segmentation," *Computer Graphics and Image Processing*, vol. 13, no. 3, pp. 222 – 241, 1980.
[31] O. Ghita, D. Ilea, A. Fernandez, and P. Whelan, "Local binary patterns versus signal processing texture analysis: a study from a performance evaluation perspective," *Sensor Review*, vol. 32, no. 2, pp. 149–162, 2012.
[32] A. Oliva and A. Torralba, "Modeling the shape of the scene: A holistic representation of the spatial envelope," *International Journal of Computer Vision*, vol. 42, no. 3, pp. 145–175, May 2001.
[33] L.-J. Li and L. Fei-Fei, "What, where and who classifying event by scene and object recognition?" in *11th International Conference in Computer Vision*, 2007, pp. 1–8.